Petroleum Science 23 (2026) 2963–2975

Contents lists available at ScienceDirect

Petroleum Science

journal homepage: www.keaipublishing.com/en/journals/petroleum-science

Original Paper

Microscopic forces between methane hydrate particle and droplet-wetted sand grain surface in a high-pressure system: Experiments and mechanisms

En Li [a], Zhi-Yuan Wang [a,b], Yue Zhang [c], Yu-Kun Guo [d], Peng-Fei Li [e], Jian-Bo Zhang [a,b,*], Qing-Wen Kong [a]

[a] School of Petroleum Engineering, China University of Petroleum (East China), Qingdao, 266580, Shandong, China
[b] Shandong Key Laboratory of Offshore Oil & Gas and Hydrates Development, Qingdao, 266580, Shandong, China
[c] West Drilling Engineering Company, CNPC, Urumqi, 830011, Xinjiang, China
[d] CNOOC China Limited, Zhanjiang Branch, Zhanjiang, 524057, Guangdong, China
[e] CNOOC China Limited, Hainan Branch, Haikou, 570100, Hainan, China

ARTICLE INFO

Article history:
Received 20 May 2025
Received in revised form
20 September 2025
Accepted 23 November 2025
Available online 29 November 2025

Edited by Teng Zhu and Min Li

Keywords:
Methane hydrate particle
Adhesion force
Pore channel
Sand
Flow assurance

ABSTRACT

Solving the issue of hydrate formation and blockage in pipelines during deepwater oil and gas development and hydrate-based green energy extraction is a crucial flow assurance safety concern. The micro-forces between hydrate particles and wetted surfaces are key parameters in studying the aggregation or detachment behavior of hydrates on pipe walls. Current research primarily focuses on carbon steel surfaces, with a lack of studies on the micro-forces between hydrates and wetted sand grain surfaces in oil and gas pipeline flow systems and hydrate extraction processes. In this study, a visual particle micro-force measurement device was designed to investigate the micro-forces between hydrates and wetted sand grain surfaces in a high-pressure system. The results showed that at subcooling degrees of 1, 3, 5, 7, and 10 °C, the micro-forces between hydrate particles and wetted sand grain surface droplets ranged from 4242.46 to 8315.27 $mN \cdot m^{-1}$. The micro-force increased by 196.88%, 217.99%, 219.92%, 209.92%, and 218.47% compared to the micro-forces between hydrate particles and wetted carbon steel surfaces. Subcooling and contact time are strong functions of the micro-force between hydrate particles and wetted sand grain surfaces. The enhancement of the micro-force on the wetted sand grain surfaces is primarily attributed to the increased supporting force provided by the hydrate shell. The increase in micro-force is governed by the superposition of multi-scale adhesion forces. Factors such as the hydrophilic nature of sand grain surfaces, pore effects, blockage of pore channels, localized pressure concentration, and mechanical interlocking effects contribute to the increased micro-force between hydrate particles and the wetted sand grain interface. This study lays a foundation for elucidating the coupling deposition mechanism of hydrates and sand grains during deepwater oil and gas production, and further provides a theoretical reference for the safe, efficient, and continuous exploitation of hydrate-based green energy.

1. Introduction

Natural gas hydrates are considered a highly promising green energy resource due to their abundant supply, high efficiency, and environmentally friendly benefits (Kong et al., 2025; Zhang et al., 2024; Chen et al., 2025; Iravani et al., 2025). Due to their enhanced energy density and clean combustion characteristics, they are regarded as an important supplementary resource in the future energy structure. Hydrates are solid compounds formed when water molecules encapsulate gas molecules (such as methane, ethane, propane, carbon dioxide, hydrogen, etc.) in a cage-like structure. Hydrates have important applications in low-carbon transport CCUS, seabed CO_2 gas sequestration, gas

* Corresponding author.
E-mail address: zhangjianbo2@163.com (J.-B. Zhang).
Peer review under the responsibility of China University of Petroleum (Beijing).

https://doi.org/10.1016/j.petsci.2025.11.042

separation, solution concentration and separation, energy utilization, refrigeration, and other areas (Sloan et al., 2008; Lee et al., 2014; Zhang et al., 2024,Wang et al., 2020a, 2020b).

However, during the development of natural gas hydrates (NGH), the secondary formation of hydrates in production pipelines is one of the major obstacles affecting extraction safety and efficiency. Additionally, ultra-deepwater oil and gas resources are considered a key strategic area for future energy supply, with huge development potential and value. In deepwater offshore exploration, oil-gas-water-solid multiphase pipelines operating under low-temperature, high-pressure conditions near the seabed mudline are prone to hydrate formation and other flow safety issues. Once hydrates form, they accumulate on the pipeline walls, reducing the flow space for fluids in the pipeline. In severe cases, this can even lead to blockages, damaging pipeline components and posing significant safety risks to deepwater oil and gas exploration and development (Jassim et al., 2010; Koh et al., 2011; Wang et al., 2017; Li et al., 2025a, 2025b). The adhesion and aggregation of hydrates are the main factors causing fluid flow resistance in pipeline transportation, and revealing the micro-forces of hydrates is crucial for studying hydrate particle aggregation and deposition (Lorenzo et al., 2014a, 2014b; Zerpa et al., 2012; Rao et al., 2013; S.L. Wang et al., 2017). In pipeline flow systems, unstable sand grains from the formation can also be carried into the flow channel with the fluid. The coexistence of hydrate particles and wetted sand grains triggers more severe hydrate-sand coupling deposition and blockage problems (Liu et al., 2017a, 2017b; Lingelem et al., 1994; Sum et al., 2012; Phan et al., 2025). A schematic diagram of the micro-forces causing hydrate and wetted sand grain deposition and blockage is displayed in Fig. 1.

Sand production is also a key technical issue that needs to be addressed during the development of methane-rich natural gas hydrates (NGH) (Chen et al., 2022; Hao et al., 2024). The transport of hydrate in an in-situ gas-water system through pipelines inevitably involves the issue of significant silt mixing. When the sand-containing decomposition water flows through areas near the seabed mudline, can promote the reformation of hydrates, causing the dissolved methane in the decomposition water to rapidly reform hydrate (Kim et al., 2022). This results in the formation of hydrates, which couple with the sand particles carried in the liquid, leading to flow path blockages and forcing the suspension of continuous natural gas hydrate extraction.

During previous field trials of natural gas hydrate production, the production process was repeatedly affected by secondary hydrate formation and sand production. For instance, in the 2012 field production test conducted in Alaska, USA, hydrate reformation led to blockage in the flare pipeline, forcing a suspension of production operations for approximately five days (Schoderbek et al., 2013). In March 2013, Japan conducted the world's first offshore production test of methane hydrates using the D/V Chikyu drilling vessel at the Daini Atsumi Knoll, at a water depth of approximately 1000 m (Sakurai et al., 2017; Konno et al., 2017). However, the test was eventually terminated due to severe sand production in the production well. In the second offshore production test conducted by Japan in 2017, after reopening the well following a shut-in operation during a typhoon, the production was interrupted twice due to secondary hydrate formation in the tubing string. The removal of hydrate blockages required 31.25 h and 13.5 h, respectively, significantly delaying the production schedule (Sakurai et al., 2017; Tao et al., 2019). Therefore, studying the micro-forces between CH_4 hydrate particles and wetted sand grain surfaces can lay the basis for addressing the hydrate-sand coupling deposition and blockage problem in pipelines, and provide theoretical support for the analysis of sand extraction issues in the safe and continuous extraction of hydrate-based green resources.

To explore the micro-forces of hydrates, scholars have designed and developed experimental devices for measuring the micro-mechanical forces of hydrates, considering all possible forms of micro-forces within the system. These mainly include the micro-forces between particles and the micro-forces between particles and wall surfaces (Brown et al., 2018; Aman et al., 2013; Morrissy et al., 2017; Lo et al., 2008; Wang et al., 2023). The micro-forces between hydrate particles are mainly studied in a cyclopentane (CyC5) system. Brown et al. (2016a, 2016b, 2018) measured the micro-force between hydrate particles in cyclopentane (at 3 °C) and found it to be approximately 4.2 $mN{\cdot}m^{-1}$. Aman et al. (2011, 2012, 2013) also found similar results under the same experimental temperature conditions, indicating that the micro-forces in the cyclopentane (CyC5) system are relatively small. Li et al. (2023)

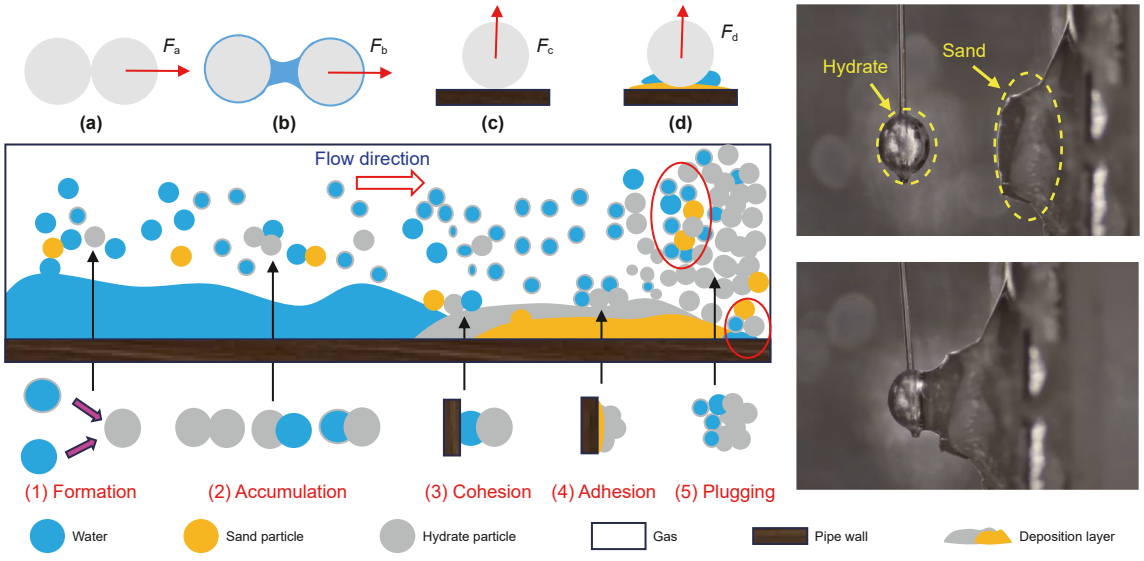

Fig. 1. Microscopic forces between hydrates and sand grains in a high-pressure flow system. (**a**) F_a denotes the micromechanical force between hydrate particles; (**b**) F_b denotes the micromechanical force between a hydrate particle, a liquid droplet, and another hydrate particle; (**c**) F_c denotes the micromechanical force between a hydrate particle and the carbon steel wall; (**d**) F_d denotes the micromechanical force between a hydrate particle and the wetted sand-grain wall.

found that the micro-force between two dry methane hydrate particles ranged from 27.24 to 35.20 $mN \cdot m^{-1}$. Zhou et al. (2023) studied wax-containing systems on the micro-forces of hydrate particles. The micro-force of hydrates in a wax-free system was 8.54 $mN \cdot m^{-1}$, while in the wax-containing system, the micro-force was 5.94 $mN \cdot m^{-1}$. Dong et al. (2020) found that the micro-force between two hydrate particles with a liquid droplet in the cyclopentane (CyC5) system was 117 $mN \cdot m^{-1}$. Liu et al. (2017a, 2017b, 2023) also obtained similar results in the cyclopentane (CyC5) system, where the micro-force was found to be 116.3 $mN \cdot m^{-1}$. The presence of liquid droplets significantly increases the micro-force of hydrate particles.

Research on the micro-forces between hydrate particles and wall surfaces can analyze the adhesion behavior of hydrate particles on pipe walls and characterize the strength of hydrate particle aggregation. It is a successful approach for evaluating the aggregation ability of hydrate deposits on pipeline walls and understanding the aggregation characteristics of hydrate particles. For experimental convenience, initial studies focused on measuring the micro-forces between hydrate particles and carbon steel surfaces in a cyclopentane (CyC5) system at atmospheric pressure (Nicholas et al., 2009; Brown et al., 2017). Aspenes et al. (2010) found that, when the subcooling degree was around 3 °C and no droplet was present, the micro-force is between 0.2 and 0.5 $mN \cdot m^{-1}$. Aspenes et al. (2010) found through experiments that when a droplet was present on the wall, this micro-force increased by two orders of magnitude, reaching 51 $mN \cdot m^{-1}$. Due to experimental limitations, research on hydrate micro-forces under high-pressure conditions is limited. Exploring micro-forces of hydrates under high pressure is more in line with actual working conditions. Liu et al. (2023) and Li et al. (2023) studied the micro-forces between hydrate particles and wetted carbon steel wall surfaces in a high-pressure methane gas system. The experiments showed that the micro-force was in the range of $\times 10^3$ $mN \cdot m^{-1}$. They also studied the reduction in micro-forces after adding hydrate inhibitors. Wang et al. (2023) found that QAs1 could reduce the micro-force of methane hydrates and proposed the mechanism of QAs1's action under different subcooling conditions. In the hydrate formation process, previous studies have shown that nanoscale sand particles dispersed in aqueous solution can promote hydrate nucleation and growth by adsorbing methane molecules and increasing the gas–liquid interfacial area (Wang et al., 2018, 2021). Sand grains play a promotive role in hydrate formation, and this effect becomes more pronounced with increasing sand particle concentration (Huang et al., 2021; Shi et al., 2022). Regarding hydrate dissociation, sand grains exhibit minimal influence on the hydrate dissociation rate. However, hydrophilic sand grains tend to adsorb at the CO_2-liquid water interface, thereby impeding the coalescence of gas bubbles during the dissociation process (Kim et al., 2022). At the same time, macroscale mechanical studies have shown that hydrate-sediment interfaces exhibit failure behaviors under shear that are significantly different from those of bulk hydrate or bulk hydrate-bearing sediments (Li et al., 2022; Zhang et al., 2024). These macroscale findings provide essential background for understanding interfacial instability and flow-assurance risks in deepwater development. Nevertheless, they cannot directly quantify the origins and evolution of interfacial adhesion forces at the single-particle scale, highlighting the need for complementary quantitative measurements at the microscale.

In summary, research on the micro-forces between hydrates and wall surfaces has primarily focused on carbon steel surfaces, which are mainly applicable to wellbores or transport pipelines used in oil and gas extraction. However, there is still a lack of systematic research on the micro-forces between secondary hydrate formation and sand particle coupling deposition during hydrate extraction. Due to the differences in properties between sand grain surfaces and pipeline carbon steel surfaces, the micro-forces between hydrate particles and these two types of surfaces differ significantly. The lack of research in this area has led to a limited understanding of this critical field in the industry, making it difficult to develop comprehensive and effective strategies for preventing and controlling hydrate blockages. Consequently, it is important to examine the micro-forces between hydrate particles and wetted sand grain surfaces to reveal the particle adhesion and deposition mechanism of hydrate-sand coupling, which will provide guidance for the safe transportation of hydrates in pipelines during the extraction of hydrate-based green energy.

2. Experimental

2.1. Experimental facility

The materials used for the micro-force experiments between methane hydrate particles and wetted sand grain surfaces in a high-pressure system include high-purity methane gas, ultrapure deionized water produced by a homemade water deionization system, rough sand grain surfaces (mainly composed of quartz, >90%), glass capillary tubes for point sampling, a digital micrometer, and a liquid phase micro-injector. The specific parameters are listed in Table 1.

To conduct research on the micro-forces of hydrate particles in a high-pressure system, a direct measurement device for the micro-forces between hydrate particles and wetted sand grain surfaces was developed, as shown in Fig. 2. This system includes four main subsystems for measuring the micro-forces: the MMF measurement device (high-speed camera with magnification of 70–450x, and an annular LED light for accurate brightness control), the data acquisition device, the temperature management device, and the gas injection pressure management device (experimental range: −20–50 °C and 0−50 MPa, experimental accuracy: 0.1 °C and 0.01 MPa) (Wang et al., 2023; Li et al., 2023; Zhang et al., 2024).

2.2. Experimental procedure

The main steps of the micro-force experiment between methane hydrate and wetted sand grain surfaces under high-pressure conditions are as follows.

(1) Preparation of wetted sand grains and hydrate particles

A fixed sand grain surface is installed at the top of a cantilever arm. Two glass capillary tubes are mounted at the moving ends of the cantilever, with the ends of the tubes containing ice particles and liquid droplets, as shown in Fig. 3(a). A three-dimensional motion platform of the microscopic operation system was used to gently place a liquid droplet onto the sand grain surface, forming a droplet-wetted sand grain surface (i.e., the sand grain surface was covered by the droplet to establish the initial wetted state). Methane gas, cooled to the system temperature, is then slowly injected at a speed of 0.01 $MPa \cdot s^{-1}$ to ensure that the temperature fluctuation inside the reaction vessel remains within a small range. Once the pressure reaches the experimental set value, gas injection is stopped. The temperature and pressure are maintained for 30 min as shown in Fig. 3(b), During this process, the ice particle surface gradually forms a hydrate shell under induced conditions, eventually completely transforming into hydrate (Wang et al., 2023).

(2) Contact process between hydrate particles and wetted sand grain surface

Table 1
Experimental material parameters table.

Materials	Parameter	Manufacturer
High-purity CH_4 gas	CH_4 Purity >99.9%	China Heng laixiang Co., Ltd.
Sand particles	Diameter: 0.8–1.2 mm	China Aladdin Co., Ltd.
Glass capillary tube for point sampling	Inner diameter: 0.9–1.1 mm	China Medical Factory
Digital micrometer	Measurement accuracy: 0.002 mm	China Heng laixiang Co., Ltd.
Liquid phase micro-injector	Specification: 1 μL	China Gaoge Industrial and Trade Co., Ltd.
Ultra-pure water	Conductivity <18 mΩ	Self-made by laboratory

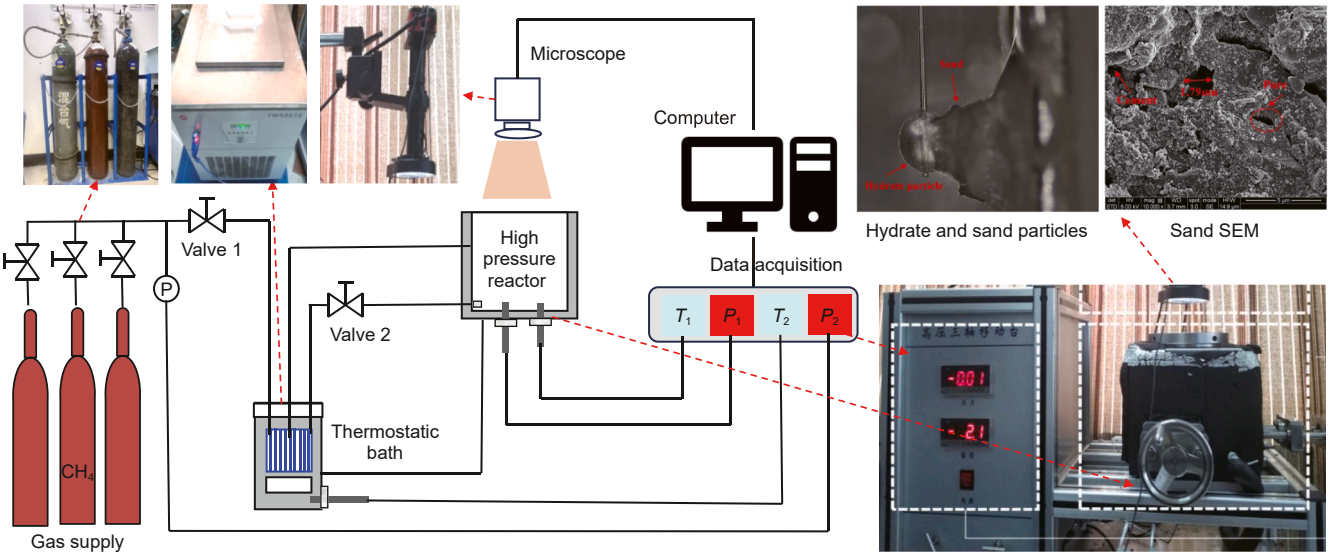

Fig. 2. The high-pressure visual micromechanical force experimental device for hydrates in the system (Wang et al., 2023; Zhang et al., 2024).

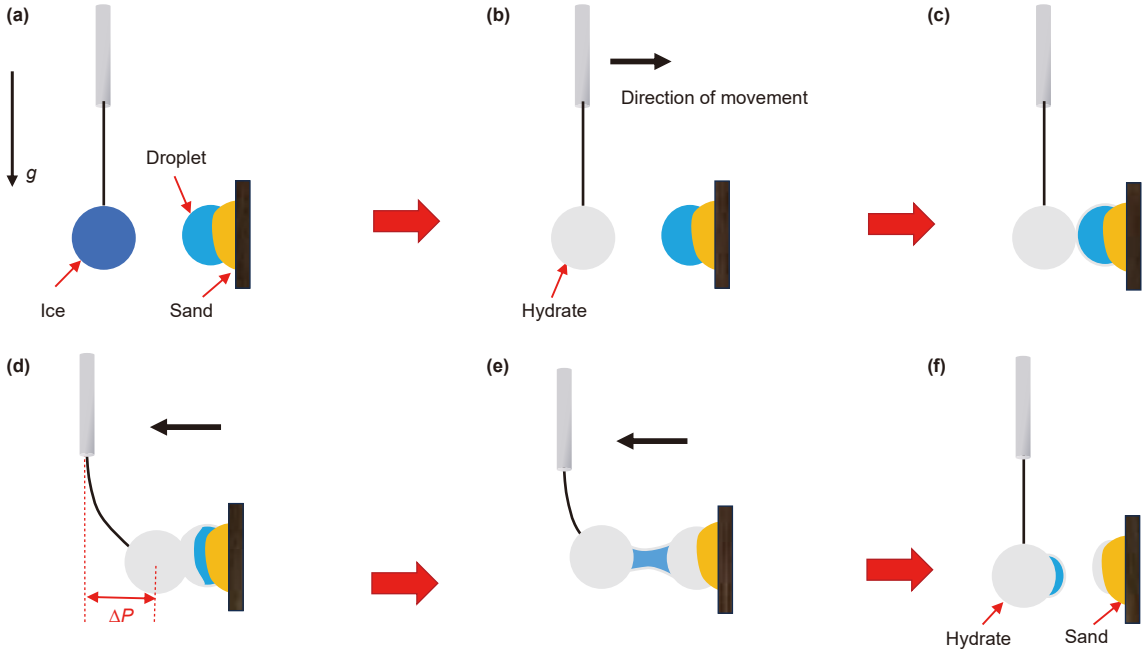

Fig. 3. Measurement method of micro-forces between hydrate particles and wetted sand grain surfaces.

Using the micro-manipulation system, the position of the wetted sand grain is fixed, and the three-dimensional movement platform controls the hydrate particle to move uniformly toward the wetted sand grain surface. When the hydrate contacts the liquid droplet on the wetted sand grain surface, its movement is continued for a short distance, as shown in Fig. 3(c) and (d).

According to the experimental requirements, the connection between the hydrate and the wetted sand grain surface is maintained for a certain amount of time. After the contact, the induced effect of the hydrate particle accelerates the transformation of the liquid droplet on the wetted sand grain surface into a hydrate.

(3) Measurement of micro-forces between hydrate particles and wetted sand grain surface

As shown in Fig. 3(e), the glass fiber at the moving end is controlled to move uniformly downward until the hydrate formed from the droplet completely detaches from the metal wall surface. The high-speed camera above records the maximum deformation of the glass fiber during the detachment process, denoted as ΔP. The specific value is processed using ImageJ software. By applying Hooke's law of elasticity, the micro-force F between the hydrate and the wetted sand grain surface is calculated (Wang et al., 2023; Li et al., 2023).

$$\begin{cases} F = k\triangle P \\ F_a = \dfrac{1}{2}F\left(\dfrac{1}{R_1}+\dfrac{1}{R_2}\right) \end{cases} \quad (1)$$

In the equation, F_a represents the normalized micro-force, k is the elasticity coefficient of the glass fiber, R_1 and R_2 are used to represent the radii of the two particles measured, the values of which were determined using the ImageJ image processing software.

As shown in Fig. 3(f), the experiment ends once the liquid bridge between the particle and the wetted sand grain surface breaks, and all experimental devices are shut down. Fig. 4 illustrates the specific process of the micro-force experiment. Based on the described experimental steps, at least 40 pull-off tests were conducted. Each experimental condition was measured repeatedly to ensure consistency, and the final experimental results were expressed as the average values. The associated error was defined using the 95% confidence interval based on the t-distribution. For each subcooling condition, deformation data of the glass fiber was obtained from three groups of stable measurements.

3. Experimental results

The core of the micro-force measurement experiment between methane hydrate particles and wetted sand grain surfaces in a high-pressure CH_4 gas system is to indirectly reflect the magnitude of the micro-forces by capturing the deformation of the glass fiber. To reveal the micro-force mechanism of hydrate particles on wetted sand grain surfaces, this study first investigates the effects of subcooling degree and contact time on micro-forces.

3.1. Effect of subcooling degree on micro-forces

Changes in temperature and pressure can cause significant differences in the micro-forces between particles. Subcooling degree is one of the key factors affecting hydrate aggregation and deposition (Yang et al., 2004; Li et al., 2023; Wang et al., 2023). The seafloor mudline temperature of deepwater gas wells typically ranges from 2 to 4 °C. In this study, the reaction chamber temperature for all micro-mechanical experiments was uniformly set to 1.7 °C. The microscopic force measurements between methane hydrate particles and droplet-wetted sand grain surfaces were conducted under pressures of 3.37, 4.13, 5.05, 6.28, and 8.47 MPa, which correspond

Table 2
Micro-force values between hydrate particles and wetted sand grain surfaces in pure water at different subcooling degrees with a contact time of 60 s.

Subcooling, °C	Micro-force, mN·m^{-1}			Average value, mN·m^{-1}
	F_a	F_b	F_c	
1	4200.35	4243.79	4283.23	4242.46
3	5100.21	5180.32	5168.98	5149.84
5	6000.22	6097.35	6085.05	6060.87
7	6900.21	6968.67	6943.68	6937.51
10	8303.47	8356.68	8285.67	8315.27

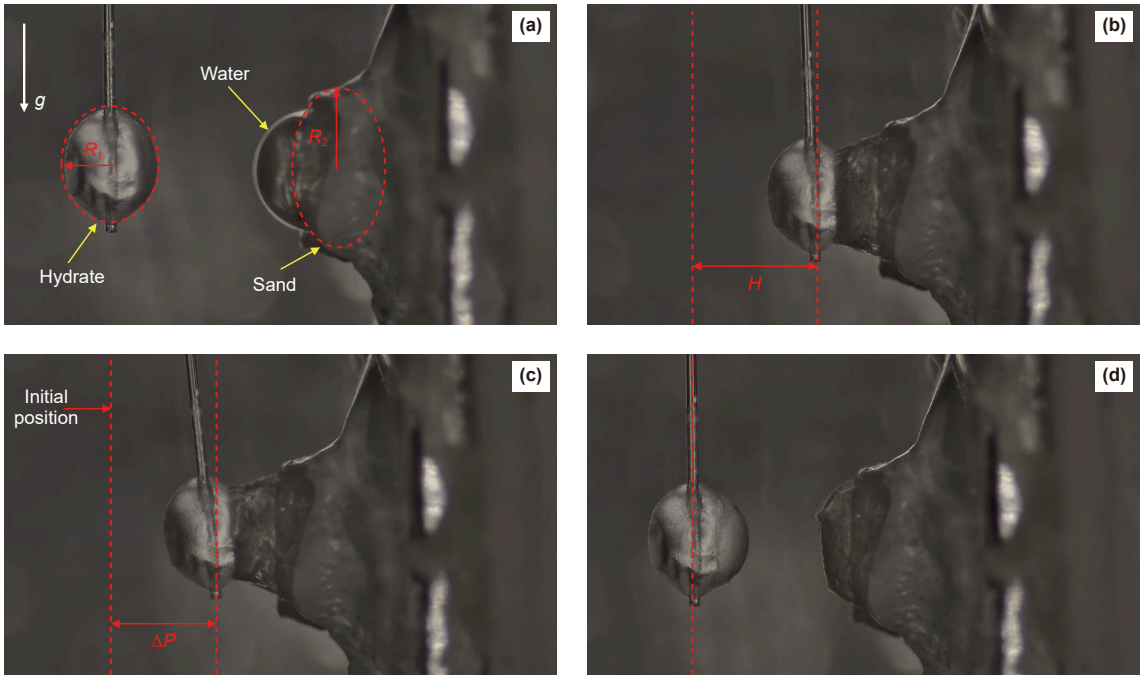

Fig. 4. Micro-force measurement process diagram between hydrate particles and wetted sand grain surfaces in a high-pressure system.

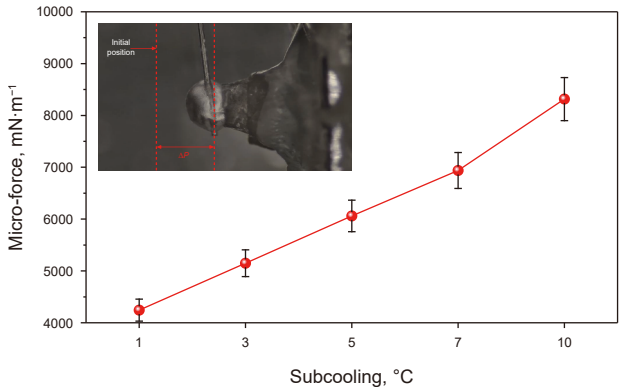

Fig. 5. Test results of the micro-force between hydrate particles and wetted sand grain surfaces (60 s).

to subcooling conditions of 1, 3, 5, 7, and 10 °C, respectively, the data are shown in Table 2. Under the set experimental conditions (contact time of 60 s), the average micro-forces between hydrate and wetted sand grain surfaces at different subcooling degrees are shown in Fig. 5. The measured micro-force values were 4242.46, 5149.84, 6060.87, 6937.52, and 8315.27 mN·m^{-1}. As the subcooling degree ranged from 1 to 10 °C, the micro-force significantly increased, approximately by 1.96 times.

In pure water, the observed increase in microscopic force between hydrate particles and droplet-wetted sand grain surfaces with rising subcooling is primarily attributed to the influence of higher subcooling on the morphology and growth pattern of the hydrate film, which alters the adhesion strength. At higher subcooling levels, hydrate nucleation and transformation occur more rapidly. Enhanced subcooling accelerates the conversion of water into hydrate, and the solidification of the liquid bridge strengthens the adhesive force, thereby increasing the measured microscopic force. Fig. 6 shows the tangential and normal growth process of the hydrate film under subcooling degrees of 1, 5, and 10 °C at time intervals of 0, 10, and 60 s. In the images, the red arc denotes the growth boundary of the hydrate film, the blue arc represents the contour of the liquid droplet on the sand grain surface, and the yellow line outlines the sand grain. Upon contact between the hydrate particle and the droplet-wetted sand grain wall, the liquid surface layer is rapidly induced to form a hydrate film. This film then quickly propagates along the droplet toward the sand grain, converting the liquid into hydrate. As the subcooling degree and contact time increase, the transparency of the formed hydrate film decreases. At higher subcooling degrees, the hydrate on the sand particles forms a fibrous, layered deposition morphology. Wang et al. (2023) and Liu et al. (2023) also observed similar fibrous deposition morphology on hydrate particles.

Under methane gas conditions, this work evaluated the micro-force between hydrate particles and wetted sand grain surfaces to range from 4242.46 to 8315.27 mN·m^{-1}. Liu et al. (2023) found that the micro-force between hydrate and carbon steel surfaces with droplets was about 1000 mN·m^{-1}. Research by Wang et al. (2023), Li et al. (2023), and others showed that this micro-force ranged from 1429.36 to 2611.61 mN·m^{-1}. A comparison of these results is shown in Fig. 7. The micro-force between hydrate particles and wetted sand grain surfaces is much higher than that between hydrate particles and wetted carbon steel surfaces. At subcooling degrees of 1, 3, 5, 7, and 10 °C, the micro-forces between hydrate particles and wetted sand grain surfaces were 4242.46, 5149.84, 6060.87, 6937.52, and 8315.27 mN·m^{-1}, respectively. These values are 196.88%, 217.99%, 219.92%, 209.92%, and 218.47% higher than the micro-forces between hydrate particles and carbon steel surfaces with droplets.

Fig. 8 illustrates the micro-images of the entire micro-force testing process. The moving end of the wall is controlled to move uniformly to the right, slowly approaching the droplet. After contact, the droplet spreads on the exterior of hydrate and sand grain under the action of interfacial tension, as shown in Fig. 8(b). Additionally, the hydrate-induced effect causes the droplet to grow toward the wetted sand grain surface, as shown in Fig. 8(f) and 8(j). The water molecule liquid film on the wetted sand grain surface sequentially induces the formation of hydrates. At higher subcooling degrees, hair-like crystals grow on the wetted sand grain surface, as shown in Fig. 8(h), 8(j), 8(k), and 8(l). Servio and Englezos (2003) and Liu et al. (2023) also found similar fibrous methane hydrate crystals under high pressure, and these fibrous methane hydrate crystals dominate the increase in micro-force.

3.2. Effect of contact time degree on micro-forces

This study further explored the effect of contact time on micro-forces. Tables 2–4 display research data for the micro-forces between hydrate particles and wetted sand grain surfaces after contact at contact times of 0, 10, and 60 s. The variation in micro-forces under different contact time conditions is shown in Fig. 9.

At the same subcooling degree, the micro-force on the wetted sand grain surface after contact times of 1, 10, and 60 s was positively correlated with contact time, but the growth rate decreased. At a subcooling degree of 10 °C, the micro-force measured after 10s of contact was about 4353.13 mN·m^{-1} higher than that after 1 s of contact, and the micro-force measured after 60 s of contact was about 2289.59 mN·m^{-1} higher than that after 10 s of contact. The increases were 260.8% and 38.1%, respectively.

This phenomenon can be attributed to a change in the dominant micro-force. Initially, the capillary force of the capillary bridge controlled the initial interaction within 1 s. Subsequently, water and gas at the water/gas interface were continuously transformed into hydrates, and the hydrate content gradually enhanced. The interaction area of the micro-force also expanded, and with the enhance in contact time, the already-formed hydrate structure became denser, resulting in an increase in micro-force. Liu et al. (2023) also observed a similar phenomenon. The growth rate slows down primarily due to the hindering effect of the hydrate shell on the mass transfer of methane molecules. As the contact time increases, the hydrate shell gradually forms and restricts the entry of external methane molecules into the shell, causing the further formation of hydrates to mainly depend on the methane molecules already dissolved in the liquid phase. The continuous consumption of CH_4 molecules in the liquid phase leads to a decrease in the micro-force growth rate.

Comparing the micro-forces between hydrate and wetted sand grain surfaces with those between hydrate and wetted carbon steel surfaces, under the same contact time and subcooling degree, the micro-force increased by 218.47% (60 s, 10 °C subcooling). This is due to the adsorption properties of the sand grains. During the experiment, as shown in Fig. 8(a–c), when the sand grain surface encounters water, the wettability of the sand grain surface ensures that the internal pores of the wetted sand grain become fully water-saturated. The water within these pores moves to the capillary bridge position as the hydrate crystals grow. Contact time is a strong function of the micro-force on the wetted sand grain surface. Therefore, under increased subcooling degree and contact time, the dominant role of micro-force gradually shifts from the capillary force of the capillary bridge to the mechanical strength of the hydrate shell.

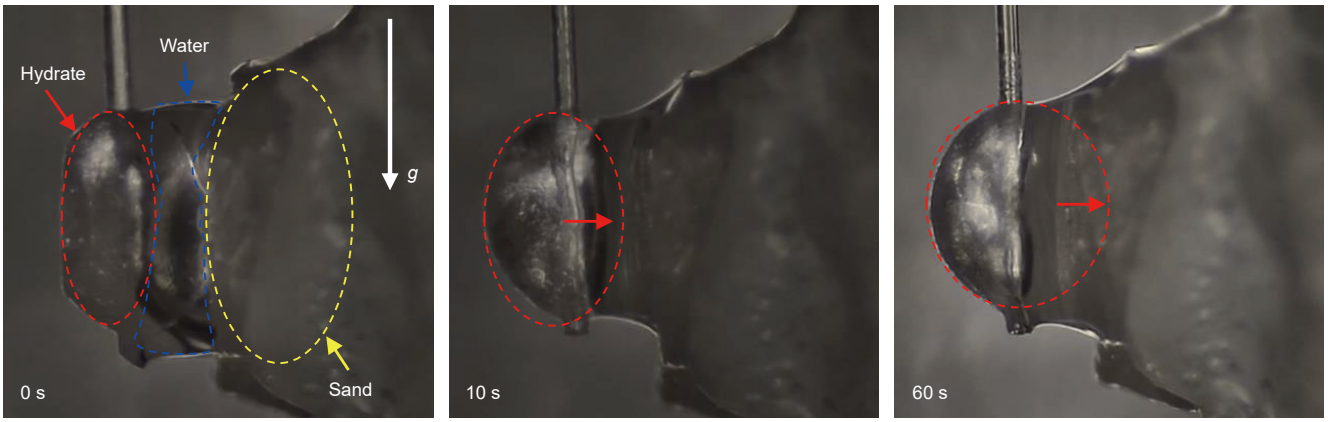

(a) Subcooling 1 °C

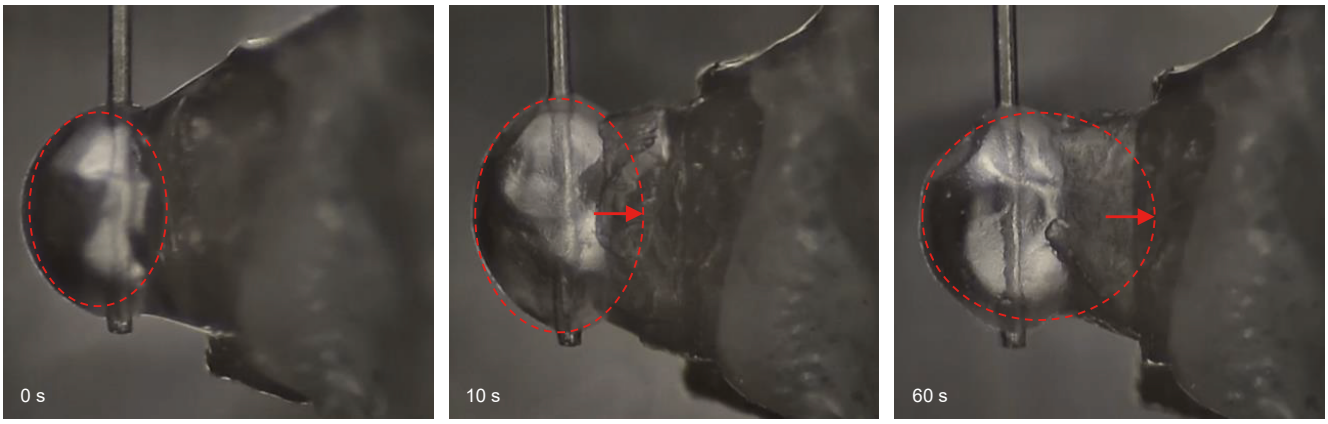

(b) Subcooling 5 °C

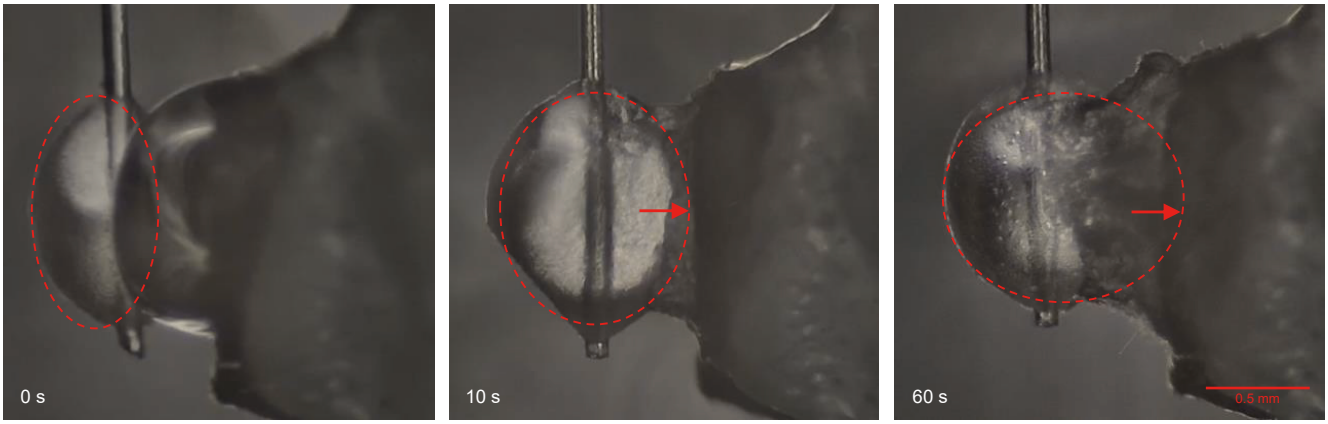

(c) Subcooling 10 °C

Fig. 6. Images of the lateral and vertical growth process of the hydrate film on the wetted sand grain surface.

4. The mechanism of micro-forces of hydrates on wetted sand grain surfaces

4.1. SEM of sand grain surface

To investigate the mechanism underlying the increase in micromechanical forces of hydrates on wetted sand-grain surfaces, a Zeiss Sigma 560 high-resolution scanning electron microscope (SEM) with a resolution of up to 1.5 nm was employed. SEM imaging at different magnifications was performed, and the micromorphology of the sand-grain specimens is presented in Fig. 10. The microscopic surface topography of the sand grain surface was analyzed based on the microstructural features of the sand grain samples.

Fig. 10(a), taken at 2000x magnification, shows that the surface of the wetted sand grain has irregular cracks and a rough surface, with many circular or irregular small holes (highlighted with yellow circles). These pore structures represent the internal pore

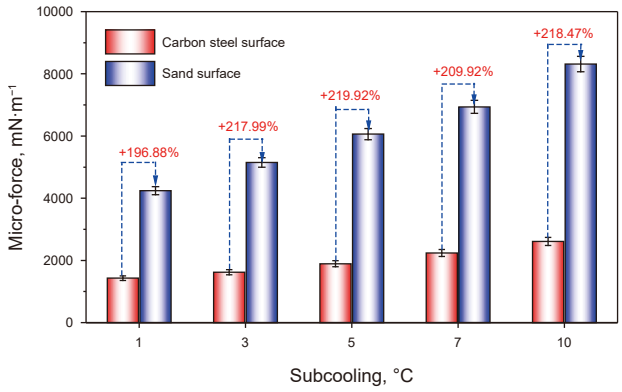

Fig. 7. Comparison of the micro-forces between hydrate particles and wetted surfaces of different materials.

Table 3
Micro-force values between hydrate particles and wetted sand grain surfaces in pure water at different subcooling degrees with a contact time of 1 s.

Subcooling, °C	Micro-force, mN·m^{-1}			Average value, mN·m^{-1}
	F_a	F_b	F_c	
1	450.29	443.56	452.54	448.80
3	700.14	710.32	719.79	710.08
5	1090.24	1103.99	1079.45	1091.23
7	1397.65	1411.45	1382.32	1397.14
10	1671.23	1668.32	1678.09	1672.55

channels of the wetted sand grain. The presence of these pores increases the interfacial area of the wetted sand grain and affects the wettability of the pore structure, making it easier to form fluid flow channels. Fig. 10(b), taken at 5000x magnification, reveals that the microstructure of the pore surface of the sand grain consists of elongated cracks or grooves with irregular edges. The

Table 4
Micro-force values between hydrate particles and wetted sand grain surfaces in pure water at different subcooling degrees with a contact time of 10 s.

Subcooling, °C	Micro-force, mN·m^{-1}			Average value, mN·m^{-1}
	F_a	F_b	F_c	
1	3200.35	3250.43	3231.32	3227.37
3	3600.20	3642.44	3658.10	3633.58
5	4100.22	4139.33	4116.64	4118.73
7	4800.24	4860.23	4837.54	4832.66
10	6000.46	6009.24	6067.35	6025.68

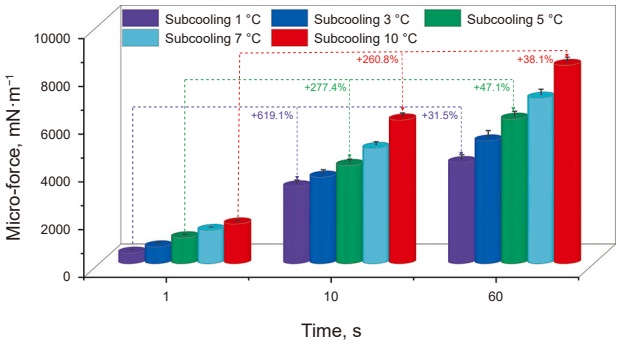

Fig. 9. Variation in the micro-force between hydrate particles and wetted sand grain surfaces under different contact time conditions.

sand grain surface has numerous pores, and the diameters of the internal pore channels vary from 1.4 to 2.4 μm. These pore characteristics significantly impact fluid flow, serving as preferential channels for gas entry, droplet seepage, and hydrate formation during the contact process. Fig. 10(c), taken at 10000x magnification, shows more detailed pores on the surface of the wetted sand grain. The areas within the yellow circles contain cementing substances. The pores and cracks are numerous and large, with a loose

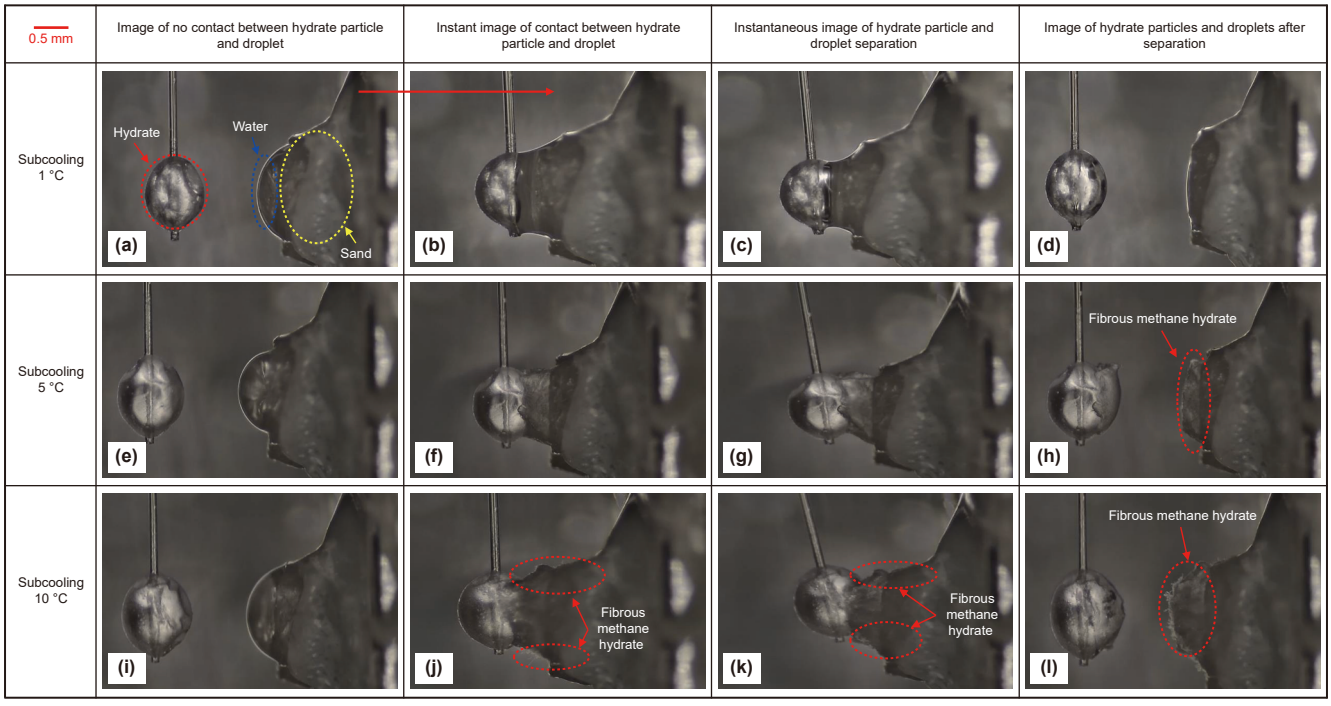

Fig. 8. Images of the micro-force measurement process between hydrate particles and wetted sand grain surfaces at different subcooling degrees.

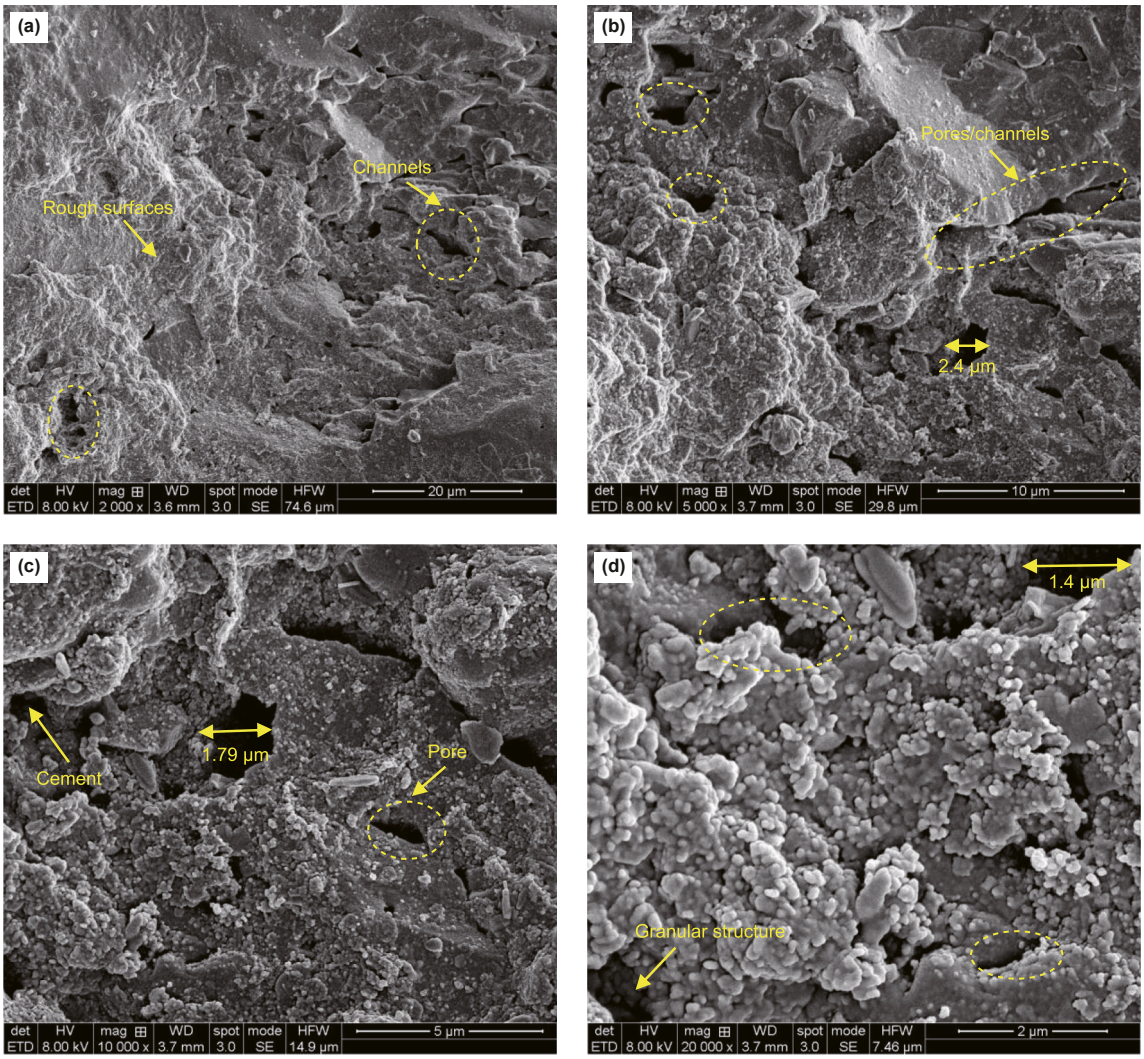

Fig. 10. SEM microscopic morphology of sand grain sample.

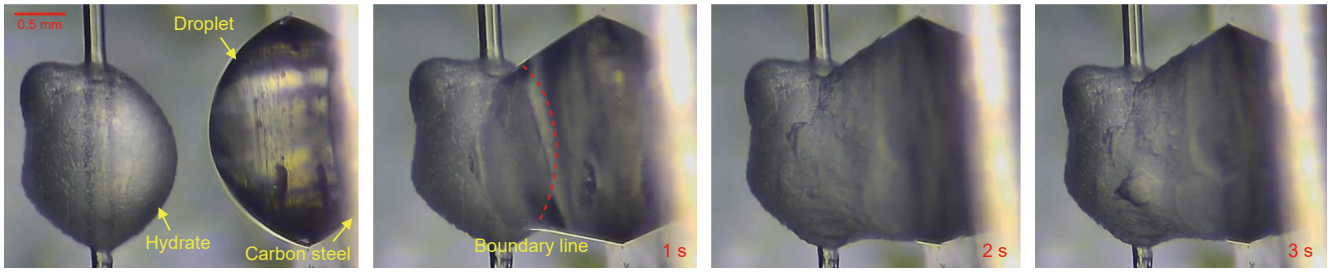

(a) Wetting carbon steel surface liquid film

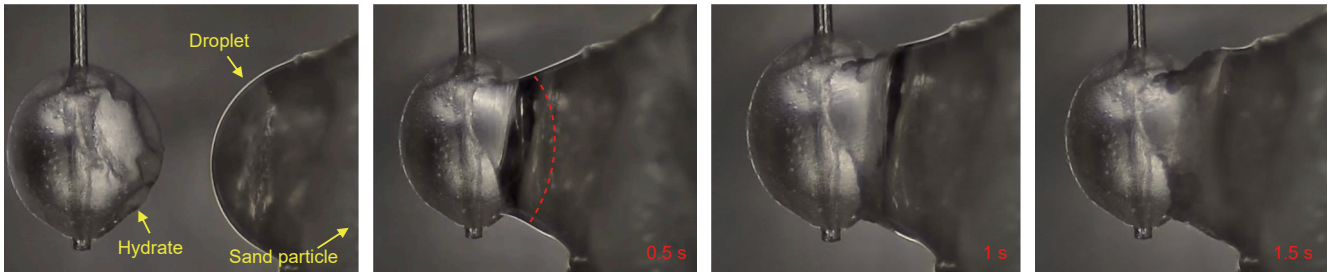

(b) Wetting sand particle surface liquid film

Fig. 11. Induced contact process of hydrate particles and wetted wall surface liquid films.

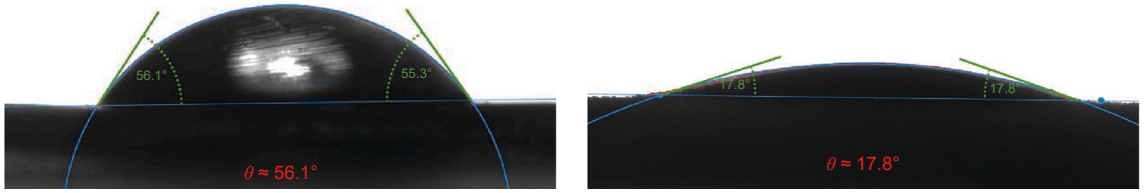

(a) Carbon steel surface **(b)** Sand particle surface

Fig. 12. Contact angle measurement images of carbon steel surface and sand particle surface.

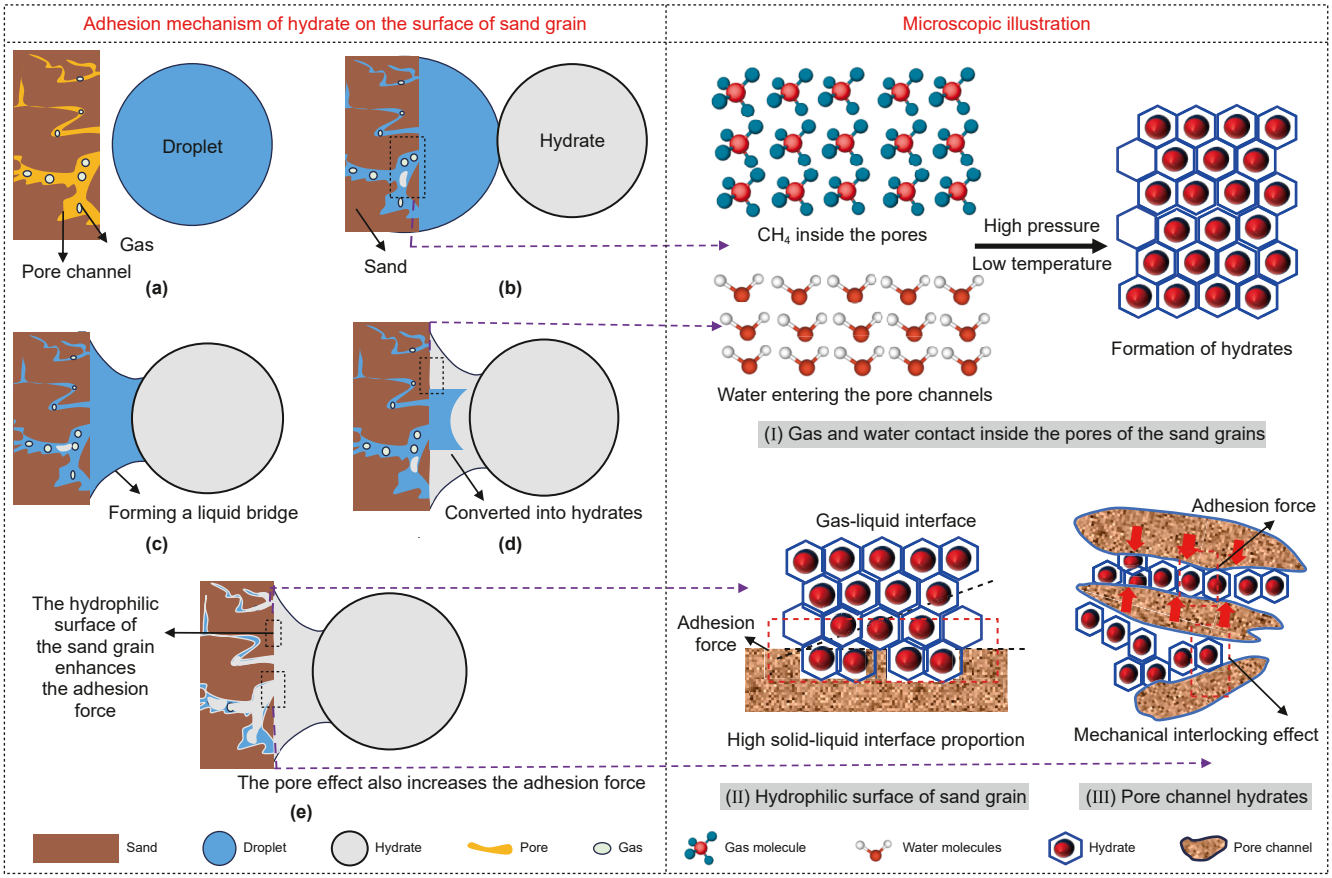

Fig. 13. The micro-force interaction mechanism and aggregation of hydrate particles on the sand grain surface. **(a)**–**(e)** Hydrate adhesion process on the sand grain surface. I: Conversion of some gas molecules and water inside the sand pores to hydrates; II: The sand grain surface exhibits superhydrophilicity, enhancing the solid–liquid interfacial force and thereby increasing the microscopic adhesion force; III: Localized pressure concentration and mechanical interlocking effects.

structure. Deep pores and complex surfaces affect the wettability angle and flow properties of the particles. Fig. 10(d), taken at 20000x magnification, reveals smaller crystals or granular structures inside the pores of the sand grain particles. These are distributed across the surface, and the irregular crystal morphology enhances the friction between the fluid particles inside the pores.

4.2. The mechanism of increased micro-forces of hydrates on wetted sand grain surfaces

The study found that due to the differences in the properties of the sand grain surface and the carbon steel pipeline wall, as shown in Fig. 7, the micro-force of the hydrate on the wetted sand grain surface significantly increases. SEM images show that the surface of the sand grains has numerous pore channels, which provide microscopic flow paths for methane gas and water.

Through the hydrate micro-force measurement experiments, the adhesion mechanism of the hydrate on the wetted sand grain surface was observed and proposed. As shown in Fig. 13(a)–13(e), based on the SEM images of the sand grain microstructure, sand grains' surface has many irregular cracks and rough surfaces, and the internal structure of the sand grains contains irregular pore channels. Before the droplet contacts the hydrate, gas molecules enter the pore channels due to pressure. Once the droplet contacts the hydrate, water molecules enter the pore channels and form a small amount of hydrate molecules with the CH_4 gas molecules, as shown in Fig. 13(a) and (b).

Fig. 11 illustrates the complete process of hydrate formation from liquid films on droplet-wetted carbon steel and sand grain surfaces, induced by contact with hydrate particles. The phase boundary between the hydrate and liquid phases during the growth process is clearly observable. Under the experimental conditions (subcooling of 10 °C), the liquid film on the carbon steel surface was fully converted into hydrate within 3 s. In contrast, the

wetted sand grain surface significantly accelerated the conversion process, with complete transformation occurring within only 1.5 s. This indicates that the presence of the sand grain wall promotes a faster conversion of the liquid bridge into hydrate. As subcooling and contact time increase, the hydrate growth rate becomes faster, thereby accelerating the solidification of the liquid bridge into a hydrate shell. On the sand grain surface, the hydrate tends to form layered accumulation morphologies, with more rapid growth as shown in Fig. 11(b).

As shown in Fig. 10(a), the irregular cracks and microvoids on the surface of the sand particles (Fig. 13(d)) contribute to the complex and irregular crack patterns, which endow the sand particle surface with good wettability. The contact angles θ of the carbon steel surface and sand particle surface were measured, as shown in Fig. 12. Both images were obtained under identical temperature conditions. The sand grain surface exhibited greater hydrophilicity compared to the carbon steel surface, allowing the liquid droplet to wet more easily and spread more extensively. This led to a larger contact area between the liquid and the sand particle surface, as well as a higher interfacial tension within the system. When a droplet comes into contact with the sand grain wall, the enhanced wettability affects both the solid-gas and solid-liquid interfacial tensions. This reinforces the hydrophilic interaction of the droplet with the sand grain surface, resulting in a true solid-liquid contact area that is significantly larger than the apparent contact area. Consequently, the proportion of the solid-liquid interface increases, which enhances the interfacial force at the solid-liquid boundary and strengthens the adhesion between the droplet and the sand grain wall.

The microscopic force between hydrate particles and the wall surface is determined by the combined effect of the liquid bridge and the hydrate shell (Wang et al., 2023; Li et al., 2023). For the case of hydrate particles interacting with wetted sand grain surfaces, additional factors must be considered—particularly the hydrate-filled pore channels where hydrate particles have either induced formation or where hydrate molecules preexist. As shown in Fig. 13(e), most of these pore channels are filled with hydrate. The presence of hydrate inside the pores primarily contributes to strengthening the microscopic force of the hydrate shell. The underlying mechanisms are as follows.

(1) Surface hydrophilicity and pore effect: The sand grain surfaces are superhydrophilic, allowing the liquid to fully spread, resulting in a high solid-liquid interfacial fraction. This increases the interfacial force at the solid-liquid boundary, thereby enhancing the adhesive force between the hydrate particle and the wetted sand grain surface. Moreover, the existence of hydrate within the pore channels increases the effective contact area on the sand grain surface. The structure of these pore channels provides favorable sites for hydrate formation and adhesion, ultimately leading to enhanced microscopic forces (Fig. 13II).
(2) Interface adhesion between hydrate in pore channels and pore walls: After hydrate forms within the pore channels, due to chemical bonding, capillary force effects, and the interlocking effect of crystal growth (Wang et al., 2020), micro-forces are generated between the hydrate and the sand grain surface (Fig. 13III).
(3) Pore channel blockage and reduced permeability: As the hydrate gradually fills the pore channels, the fluid permeability of the channels decreases, concentrating fluid pressure in limited areas. This localized pressure concentration effect further increases the micro-force between the hydrate in the sand grain pore channel and the pore channel wall (Fig. 13III).
(4) Formation of a connection network between hydrate in pore channels and hydrate shell: Hydrates within the sand grain pores form a network connection with the hydrate shell through liquid water films and crystal expansion. This network connection increases the micro-force to the entire wetted sand grain surface and hydrate particle system (Fig. 13(e)). In conclusion, the mechanism for the increased micro-force of hydrates on wetted sand grain surfaces is the superimposed effect of multi-scale micro-forces, which increases the force provided by the hydrate shell.

5. Conclusions

This study, based on a self-developed high-pressure visualization micro-force device, for the first time carried out micro-force measurements between CH_4 hydrate particles and wetted sand grain surfaces in high-pressure system. Additionally, the mechanism behind the increase in micro-forces of hydrates on wetted sand grain surfaces was revealed.

The study on the micro-forces between hydrate particles and wetted sand grain surfaces in a high-pressure system showed that the micro-forces between hydrate particles and wetted sand grain surfaces ranged from 4242.46 to 8315.27 $mN{\cdot}m^{-1}$, significantly higher than the micro-forces between hydrate particles and carbon steel surfaces with droplets. At subcooling degrees of 1, 3, 5, 7, and 10 °C, the micro-force increased by 196.88%, 217.99%, 219.92%, 209.92%, and 218.47%, respectively, compared to the micro-forces between hydrate particles and wetted carbon steel surfaces. Both increasing subcooling degree and contact time lead to an increase in the micro-force between hydrate particles and wetted sand grain surfaces.

The mechanism underlying the microscopic force between hydrates and wetted sand grain surfaces was investigated. It was found that the presence of sand grain walls accelerated the transformation of the liquid film into hydrates, and enhanced the force contributed by the hydrate shell. The increase in microscopic force is attributed to the synergistic effect of multiscale adhesion mechanisms. The hydrophilic nature of sand grain surfaces enhances the solid-liquid interfacial interaction, while the pore-scale effect improves the interfacial adhesion between hydrate formed within pore channels and the surrounding pore walls. Pore channel blockage and reduced permeability result in localized pressure concentration and mechanical interlocking effects between hydrates and pore structures, further strengthening the networked adhesion between pore-scale hydrates and the hydrate shell. As a result, the microscopic force between hydrate particles and wetted sand grain surfaces increases. Therefore, hydrate agglomerates adsorbed with sand grains exhibit stronger microscopic interactions, leading to a higher risk of blockage due to hydrate-sand coupling aggregation. These experimental data contribute to a better understanding of the gas-water-sand hydrate deposition mechanism, and provide valuable insights into the hydrate-sand coupled deposition and potential issues of secondary hydrate formation and sand production during deepwater oil and gas exploitation.

CRediT authorship contribution statement

En Li: Writing – original draft, Visualization, Software, Data curation. **Zhi-Yuan Wang:** Supervision, Investigation, Funding acquisition. **Yue Zhang:** Data curation. **Yu-Kun Guo:** Data curation.

Peng-Fei Li: Visualization, Software, Investigation, Data curation. **Jian-Bo Zhang:** Writing – review & editing, Visualization, Supervision, Methodology. **Qing-Wen Kong:** Software, Data curation.

Data availability

Data will be made available on request.

Declaration of competing interest

The authors declare that they have no known competing financial interests or personal relationships that could have appeared to influence the work reported in this paper.

Acknowledgement

The work was supported by National Science and Technology Major Project (2025ZD1403206), the National Natural Science Foundation of China (52304016), the Fundamental Research Funds for the Central Universities (24CX10004A, 25CX06003A), the Special Funds of the Taishan Scholars Program, Program for Scientific Research Innovation Team of Young Scholar in Colleges and Universities of Shandong Province (2024KJH131, 2022KJ069).

References

Aman, Z., Brown, E., Sloan, E., Sum, A., Koh, C., 2011. Interfacial mechanisms governing cyclopentane clathrate hydrate adhesion/cohesion. Phys. Chem. Chem. Phys. 13 (44), 19796–19806. https://doi.org/10.1039/C1CP21907C.

Aman, Z., Joshi, S., Sloan, E., Sum, A., Koh, C., 2012a. Micromechanical cohesion force measurements to determine cyclopentane hydrate interfacial properties. J. Colloid Interface Sci. 376 (1), 283–288. https://doi.org/10.1016/j.jcis.2012.03.019.

Aman, Z., Sloan, E., Sum, A., Koh, C., 2012b. Lowering of clathrate hydrate cohesive forces by surface active carboxylic acids. Energy Fuels 26 (8), 5102–5108. https://doi.org/10.1021/ef300707u.

Aman, Z., Olcott, K., Pfeiffer, K., Sloan, E., Sum, A., Koh, C., 2013. Surfactant adsorption and interfacial tension investigations on cyclopentane hydrate. Langmuir 29 (8), 2676–2682. https://doi.org/10.1021/la3048714.

Aspenes, G., Dieker, L., Aman, Z., Høiland, S., Sum, A., Koh, C., Sloan, E., 2010. Adhesion force between cyclopentane hydrates and solid surface materials. J. Colloid Interface Sci. 343 (2), 529–536. https://doi.org/10.1016/j.jcis.2009.11.071.

Brown, E., Koh, C., 2016a. Micromechanical measurements of the effect of surfactants on cyclopentane hydrate shell properties. Phys. Chem. Chem. Phys. 18 (1), 594–600. https://doi.org/10.1039/C5CP06071K.

Brown, E., Koh, C., 2016b. Competitive interfacial effects of surfactant chemicals on clathrate hydrate particle cohesion. Energy & Fuels 30 (10), 8065–8071. https://doi.org/10.1021/acs.energyfuels.6b00145.

Brown, E., Hu, S., Wang, S., Wells, J., Nakatsuka, M., Veedu, V., Koh, C., 2017. Low-adhesion coatings as a novel gas hydrate mitigation strategy. In: Offshore Technology Conference. https://doi.org/10.4043/27874-MS.

Brown, E., Hu, S., Wells, J., Wang, X., Koh, C., 2018. Direct measurements of contact angles on cyclopentane hydrates. Energy & Fuels 32 (6), 6619–6626. https://doi.org/10.1021/acs.energyfuels.8b00803.

Chen, H.E., Du, H., Shi, B., Shan, W.C., Hou, J.Q., 2022. Mechanical properties and strength criterion of clayey sand reservoirs during natural gas hydrate extraction. Energy 242, 122526. https://doi.org/10.1016/j.energy.2021.122526.

Chen, Z.R., Farhadian, A., Naeiji, P., Martyushev, D., Chen, C., 2025. Molecular-level insights into kinetic and agglomeration inhibition mechanisms of structure I and II gas hydrate formation. Chem. Eng. J. 511, 162194. https://doi.org/10.1016/j.cej.2025.162194.

Dong, S.B., Li, M.Z., Liu, C.W., Zhang, J., Chen, G., 2020. Bio-inspired superhydrophobic coating with low hydrate adhesion for hydrate mitigation. JBE 17 (5), 1019–1028. https://doi.org/10.1007/s42235-020-0085-5.

Hao, Y.M., Wang, C.M., Tao, S., Sun, Y.Q., Liu, R., Liang, J.K., 2024. Effect of sand production on physical properties and fracturing development of gas hydrate reservoir. Energy 288, 129838. https://doi.org/10.1016/j.energy.2023.129838.

Huang, X.Z., Ma, G.Y., Wang, P., 2021. Effect of nanofluid and SDS compound system on natural gas hydrate formation. Petrol. Sci. Technol. 39 (17–18), 666–682. https://doi.org/10.1080/10916466.2021.1967387.

Iravani, D., Farhadian, A., Sharifi, R., Berisha, A., Rahimi, A., Shaabani, A., Akbarinezhad, E., 2025. Fabrication of novel Arabic gum-grafted-polyurethanes as eco-friendly corrosion inhibitors for carbon steel in sour environments: surface analysis and inhibition mechanism. Corros. Sci. 246, 112712. https://doi.org/10.1016/j.corsci.2025.112712.

Jassim, E., Abdi, M., Muzychka, Y., 2010. A new approach to investigate hydrate deposition in gas-dominated flowlines. J. Nat. Gas Sci. Eng. 2 (4), 163–177. https://doi.org/10.1016/j.jngse.2010.05.005.

Kim, S., Zadeh, A., Nole, M., Daigle, H., Huh, C., Kim, I., 2022. Spontaneous generation of stable CO_2 emulsions via the dissociation of nanoparticle-aided CO_2 hydrate. J. Petrol. Sci. Eng. 208, 109203. https://doi.org/10.1016/j.petrol.2021.109203.

Koh, C., Sloan, E., Sum, A., Wu, D., 2011. Fundamentals and applications of gas hydrates. Annu. Rev. Chem. Biomol. Eng. 2 (1), 237–257. https://doi.org/10.1146/annurev-chembioeng-061010-114152.

Kong, Q.W., Wang, Z.Y., Pei, J.H., Zhong, J., Zhang, J.B., Tong, S.K., Sun, B.J., 2025. An improved high-efficiency anti-agglomerant for avoiding hydrate flow barriers in high water-cut systems: flowloop investigation and mechanisms. Sci. China Chem. 68 (6), 2691–2711. https://doi.org/10.1007/s11426-024-2371-9.

Konno, Y., Fujii, T., Sato, A., Akamine, K., Naiki, M., Masuda, Y., Nagao, J., 2017. Key findings of the world's first offshore methane hydrate production test off the coast of Japan: Toward future commercial production. Energy & Fuels 31 (3), 2607–2616. https://doi.org/10.1021/acs.energyfuels.6b03143.

Lee, B., Koh, C., Sum, A., 2014. Development of a high pressure micromechanical force apparatus. Rev. Sci. Instrum. 85 (9), 095120. https://doi.org/10.1063/1.4896661.

Li, Y.L., Yu, G.G., Xu, M., Ou, W.J., Niu, C.C., Jiang, H.Y., Sun, J.S., 2022. Interfacial strength between ice and sediment: A solution towards fracture-filling hydrate system. Fuel 330, 125553. https://doi.org/10.1016/j.fuel.2022.125553.

Li, P.F., Tong, S.K., Pei, J.H., Zhang, J.B., Guo, Y.K., Liu, X., Wang, Z.Y., 2023. Investigation on microscopic forces between methane hydrate particles in gas phase dominated system. Fuel 350, 128776. https://doi.org/10.1016/j.fuel.2023.128776.

Li, E., Wang, Z.Y., Guo, Y.K., Zhang, J.B., Bi, S.K., Sun, B.J., 2025a. Research on the synergistic inhibition of wax formation in shale oil system using efficient wax inhibitors: Experiments and mechanisms. Chem. Eng. Sci., 121902 https://doi.org/10.1016/j.ces.2025.121902.

Li, E., Wang, Z.Y., Zhang, J.B., Pei, J.H., Li, Z.Q., Sui, X.A., Sun, B.J., 2025b. Numerical simulation study on flow aggregation characteristics of hydrate slurry in Z-Shaped pipeline. In: International Conference on Offshore Mechanics and Arctic Engineering, Volume 6: Offshore Geotechnics; Petroleum Technology. Vancouver, British Columbia, Canada. https://doi.org/10.1115/OMAE2025-156554.

Lingelem, M., Majeed, A., Stange, E., 1994. Industrial experience in evaluation of hydrate formation, inhibition, and dissociation in pipeline design and operation. Ann. N. Y. Acad. Sci. 715 (1), 75–93. https://doi.org/10.1111/j.1749-6632.1994.tb38825.x.

Liu, C.W., Geng, K.L., Dong, S.B., Li, M.Z., 2017a. Effects of Sorbitan monooleate on the interactions between cyclopentane hydtate particles and water droplets. In: Proceedings of the 6th International Conference on Informatics, Environment, Energy and Applications, pp. 1–5. https://doi.org/10.1145/3070617.3070619.

Liu, C.W., Li, Y.X., Wang, W.Y., Dong, S.B., Li, M.Z., 2017b. Modeling the micromechanical interactions between clathrate hydrate particles and water droplets with reducing liquid volume. Chem. Eng. Sci. 163, 44–55. https://doi.org/10.1016/j.ces.2017.01.031.

Liu, C.W., Zhou, C.R., Li, M.Z., Tong, S.K., Qi, M.H., Wang, Z.Y., 2023. Direct measurements of the interactions between methane hydrate particle-particle/droplet in high pressure gas phase. Fuel 332, 126190. https://doi.org/10.1016/j.fuel.2022.126190.

Lo, C., Zhang, J.S., Somasundaran, P., Lu, S., Couzis, A., Lee, J., 2008. Adsorption of surfactants on two different hydrates. Langmuir 24 (22), 12723–12726. https://doi.org/10.1021/la802362m.

Lorenzo, M., Aman, Z., Sanchez Soto, G., Johns, M., Kozielski, K., May, E., 2014a. Hydrate formation in gas-dominant systems using a single-pass flowloop. Energy & Fuels 28 (5), 3043–3052. https://doi.org/10.1021/ef500361r.

Lorenzo, M., Aman, Z., Kozielski, K., Norris, B., Johns, M., May, E., 2014b. Under-inhibited hydrate formation and transport investigated using a single-pass gas-dominant flowloop. Energy & Fuels 28 (11), 7274–7284. https://doi.org/10.1021/ef501609m.

Morrissy, S., McKenzie, A., Graham, B., Johns, M., May, E., Aman, Z., 2017. Reduction of clathrate hydrate film growth rate by naturally occurring surface active components. Energy & Fuel 31 (6), 5798–5805. https://doi.org/10.1021/acs.energyfuels.6b02942.

Nicholas, J., Dieker, L., Sloan, E., Koh, C., 2009. Assessing the feasibility of hydrate deposition on pipeline walls adhesion force measurements of clathrate hydrate particles on carbon steel. J. Colloid Interface Sci. 331 (2), 322–328. https://doi.org/10.1016/j.jcis.2008.11.070.

Phan, A., Farhadian, A., Iravani, D., Soleimani, M., Li, S., Rahimi, A., Zhao, X., 2025. Renewable oilfield reagents with multiple flow-assurance actions: Oleic acid–derived compounds inhibit gas hydrate agglomeration and corrosion. Energy 315, 134368. https://doi.org/10.1016/j.energy.2025.134368.

Rao, I., Koh, C., Sloan, E., Sum, A., 2013. Gas hydrate deposition on a cold surface in water-saturated gas systems. Ind. Eng. Chem. Res. 52 (18), 6262–6269. https://doi.org/10.1021/ie400493a.

Sakurai, S., Nishioka, I., Matsuzawa, M., Matzain, B., Goto, A., Lee, J., 2017. Issues and challenges with controlling large drawdown in the first offshore methane-hydrate production test. SPE Prod. Oper. 32 (4), 500–516. https://doi.org/10.2118/182230-PA.

Schoderbek, D., Farrell, H., Howard, J., Raterman, K., Silpngarmlert, S., Martin, K., Klein, P., 2013. Conocophillips Gas Hydrate Production Test. ConocoPhillips Co., Houston, TX (United States).

Servio, P., Englezos, P., 2003. Morphology of methane and carbon dioxide hydrates formed from water droplets. AIChE J. 49 (1), 269–276. https://doi.org/10.1002/aic.690490125.

Shi, B.H., Chen, Y.C., Wang, X.F., Song, S.F., Fu, S.K., Zhou, J.W., Gong, J., 2022. Flowloop investigation into hydrate formation and slurry flow in the presence of micron-sized sand particles. J. Petrol. Sci. Eng. 212, 110251. https://doi.org/10.1016/j.petrol.2022.110251.

Sloan, E., Koh, C., 2008. Clathrate Hydrates of Natural Gases. CRC, Boca Raton, FL.

Sum, A.K., Koh, C.A., Sloan, E., 2012. Developing a comprehensive understanding and model of hydrate in multiphase flow: From laboratory measurements to field applications. Energy & Fuels 26 (7), 4046–4052. https://doi.org/10.1021/ef300191e.

Tao, Y., Guan, G.Q., Abudula, A., 2019. Production performance and numerical investigation of the 2017 offshore methane hydrate production test in the nankai trough of Japan. Appl. Energy 251, 113338. https://doi.org/10.1016/j.apenergy.2019.113338.

Wang, S.L., Hu, S.J., Brown, E., Nakatsuka, M., Zhao, J.F., Yang, M.J., Koh, C., 2017. High pressure micromechanical force measurements of the effects of surface corrosion and salinity on CH_4/C_2H_6 hydrate particle–surface interactions. Phys. Chem. Chem. Phys. 19 (20), 13307–13315. https://doi.org/10.1039/C7CP01584D.

Wang, Z.Y., Zhang, J.B., Sun, B.J., Chen, L.T., Zhao, Y., Fu, W.Q., 2017. A new hydrate deposition prediction model for gas-dominated systems with free water. Chem. Eng. Sci. 163, 145–154. https://doi.org/10.1016/j.ces.2017.01.030.

Wang, R., Sun, H., Xu, X., Zhang, J., Wang, J., Yang, Z., Jiang, G., 2018. Study of the mechanism of hydrate formation promoted by hydrophobic nano-SiO_2. Energy Sources, Part A Recovery, Util. Environ. Eff. 40 (19), 2257–2264. https://doi.org/10.1080/15567036.2018.1477879.

Wang, H., Jin, K., Tao, J., 2020. Improving the interfacial shear strength of carbon fibre and epoxy via mechanical interlocking effect. Compos. Sci. Technol. 200, 108423. https://doi.org/10.1016/j.compscitech.2020.108423.

Wang, S.L., Fan, S.S., Lang, X.M., Wang, Y.H., Wang, P.F., 2020a. Particle size dependence of clathrate hydrate particle cohesion in liquid/gaseous hydrocarbons. Fuel 259, 116201. https://doi.org/10.1016/j.fuel.2019.116201.

Wang, W., Huang, Q.Y., Hu, S.J., Zhang, P., Koh, C., 2020b. Influence of wax on cyclopentane clathrate hydrate cohesive forces and interfacial properties. Energy & Fuels 34 (2), 1482–1491. https://doi.org/10.1021/acs.energyfuels.9b03543.

Wang, L.Y., Lu, X.R., Xu, Y.L., 2021. Experiment investigation of SiO_2 containing amino groups as a kinetic promoter for CO_2 hydrates. ACS Omega 6 (30), 19748–19756. https://doi.org/10.1021/acsomega.1c02440.

Wang, Z.Y., Li, P.F., Tong, S.K., Zhang, J.B., Zhou, C.R., Pei, J.H., Liu, C.W., 2023. Investigation on the reduction effect of QAs1 on the adhesion force between methane hydrate particles and wall droplets. Fuel 340, 127521. https://doi.org/10.1016/j.fuel.2023.127521.

Yang, S.O., Kleehammer, D., Huo, Z.X., Sloan, E., Miller, K., 2004. Temperature dependence of particle–particle adherence forces in ice and clathrate hydrates. J. Colloid Interface Sci. 277 (2), 335–341. https://doi.org/10.1016/j.jcis.2004.04.049.

Zerpa, L., Aman, Z., Joshi, S., Rao, I., Sloan, E., Koh, C., Sum, A., 2012. Predicting hydrate blockages in oil, gas and water-dominated systems. In: Offshore Technology Conference. https://doi.org/10.4043/23490-MS. OTC–23490.

Zhang, Y.J., Li, Y.L., Chen, M.T., Dong, L., Jiang, Z.Y., Shen, K.X., Wu, N.Y., 2024. Experimental study on direct shear properties and shear surface morphologies of hydrate-bearing sediments. Gas Sci. Eng. 128, 205387. https://doi.org/10.1016/j.jgsce.2024.205387.

Zhang, J.B., Li, P.F., Liu, S.J., Xu, Y.L., Tong, S.K., Wang, Z.Y., Sun, B.J., 2024. Experimental study on effects of non-ionic anti-agglomerants in preventing deposition of hydrate particles microscopically and macroscopically. Chem. Eng. Sci. 284, 119538. https://doi.org/10.1016/j.ces.2023.119538.

Zhou, S.D., Ren, Z.H., Guo, Y., Zhou, W.R., Liu, Y., 2023. Effect of wax on cohesive behavior of gas hydrate under high pressure. Energy & Fuels 37 (7), 5303–5311. https://doi.org/10.1021/acs.energyfuels.2c04379.